Rapid #: -20191239

CROSS REF ID: **2149161**

LENDER: **LSD :: Main Library**

BORROWER: **WAU :: Suzzallo Library**

TYPE:	Article CC:CCG
JOURNAL TITLE:	Carbon letters
USER JOURNAL TITLE:	CARBON LETTERSCARBON LETTERS
ARTICLE TITLE:	Effect of oxidizing treatment on electrocatalytic activity of boron-doped amorphous carbon thin films
ARTICLE AUTHOR:	Wang, Chen-Song
VOLUME:	29
ISSUE:	5
MONTH:	
YEAR:	2019
PAGES:	487-495
ISSN:	1976-4251
OCLC #:	

Processed by RapidX: 1/31/2023 4:13:16 AM

Carbon Letters (2019) 29:487–495
https://doi.org/10.1007/s42823-019-00053-9

Online ISSN 2233-4998
Print ISSN 1976-4251

ORIGINAL ARTICLE

Effect of oxidizing treatment on electrocatalytic activity of boron-doped amorphous carbon thin films

Chen-Song Wang[1] · Ni Suo[1] · Hao Huang[1] · Ai-min Wu[1] · Guo-Zhong Cao[1,2] · Gui-Feng Zhang[1]

Received: 18 December 2018 / Accepted: 8 February 2019 / Published online: 20 May 2019

Abstract
Boron-doped amorphous carbon (BDAC) thin films with a regular oxygen reduction reaction (ORR) catalytic activity were synthesized in a hot filament chemical vapor deposition device using a mixture of CH_4 and H_2 as a gas source and B_2O_3 as a boron source and then oxidized in air at 380–470 °C for 15–75 min. Scanning electron microscope, transmission electron microscope, Raman spectroscopy, X-ray photoelectron spectroscopy, and electrochemical tests were used to characterize the physical and electrochemical properties of the BDAC catalysts. It was concluded that the BDAC catalyst oxidized at 450 °C for 45 min showed the best ORR catalytic activity in alkaline medium. The oxygen reduction potential and the transfer electron number *n*, respectively, are − 0.286 V versus Ag/AgCl and 3.24 from the rotating disk electrode experiments. The treated carbon film has better methanol resistance and stability than the commercial Pt/C catalyst.

Keywords Amorphous carbon film · Electrocatalyst · Hot filament CVD · Oxidizing treatment

1 Introduction

Research and development of new energy sources are an effective way to solve energy crisis and environmental pollution [1, 2]. Due to high energy efficiency and environmental friendliness, fuel cells have received extensive attention from researchers around the world [3]. However, the fuel cells still cannot be commercialized on a large scale due to a high cost and a poor durability from the platinum-based cathode catalytic materials [4, 5]. Therefore, finding catalyst materials with strong catalytic activity, good stability, and low cost has become a key to solve the commercialization of the fuel cells.

In recent decades, a large number of non-noble-based catalysts have been proposed, including low-platinum alloys [6], metal oxides [7, 8], metal macrocyclic compound-based catalysts [9], related and doped carbon materials [10–13], and so on. In particular, doped carbon materials have become ideal candidate to replace noble metal platinum owing to excellent conductivity, good oxygen reduction reaction (ORR) catalytic activity, easy surface modification, low cost, good stability, and incapability of CO and methanol poisoning [14, 15]. However, the catalytic activity of carbon-doped materials as commercial catalysts has still room for further improvement. An effective way to improve the catalytic performance is to increase the specific surface area that has the active sites. There are many ways to increase the specific surface area of materials, such as porous structure [16], plasma etching [17], and annealing treatment [18, 19]. Though the creation of a porous structure and plasma treatment can effectively increase the specific surface area of the catalytic materials, the two methods are complicated in process and high in cost. Annealing treatment relatively is simple, and the specific surface area can be improved and controlled. Wiener et al. [18] found that the pore size of amorphous carbon has changed after annealing at 800–2000 °C in argon by analyzing the macroscopic and microscopic structure of amorphous carbon. Gokuladeepan et al. [19] treated graphene oxide composites at 300–500 °C in the atmosphere and analyzed the effects of annealing temperature on surface morphology and ORR catalytic performance. However, the researches above are not systematic and the effect laws were not established between the

✉ Gui-Feng Zhang
gfzhang@dlut.edu.cn

[1] Key Laboratory of Materials Modification by Laser, Ion and Electron Beams (Ministry of Education), School of Materials Science and Engineering, Dalian University of Technology, Dalian 116024, China

[2] Department of Materials Science and Engineering, University of Washington, Seattle, WA 98195, USA

annealing parameters and the performance. The direct air oxidation relatively is not only simple in equipment, convenient in operation, low in cost, but also capable of increasing the specific surface area of the carbon thin film.

In this work, boron-doped amorphous carbon (BDAC) films were deposited by hot filament chemical vapor deposition (HFCVD) and heat-treated in the atmosphere. The influence of the air oxidation parameters on the electrochemical properties has been investigated to further enhance the ORR catalytic activity.

2 Experimental

2.1 Preparation of BDAC films

The substrate used in this experiment was a (100) high-purity polished silicon wafer with 14×14 mm^2. The substrates were scratched using diamond paste to increase the nucleation site and then ultrasonically cleaned in acetone, ethanol, and deionized water for 10 min, respectively. The BDAC films were grown in a HFCVD device. Gas source was a CH_4/H_2 gas mixture with a flow ratio of 1/100, and boron source was a solid B_2O_3. Ta filament was located 5 mm above the substrate. During the deposition, the temperature of the filament and the substrate was maintained at about 2200 °C and 800 °C, respectively. The deposition pressure was 5.33 kPa and deposition time 6 h. The prepared BDAC films were oxidized in air using a box annealing furnace at a heating rate of 15 °C/min. The process parameters were the oxidation temperature at 380 °C, 400 °C, 430 °C, 450 °C, and 470 °C for 1 h and at 450 °C for 15 min, 30 min, 45 min, 60 min, and 75 min, respectively. The oxidized samples were then cooled slowly to room temperature in the furnace.

2.2 Characterization

The surface morphology of the BDAC films was observed by scanning electron microscope (SEM, Zeiss Supra 55) and transmission electron microscope (TEM, Tecnai G220 S-Twin). The microstructure was analyzed using a Raman spectrometer (Renishaw Invia) with a wavelength of 532 nm in the wave number range of 1000–2000 cm^{-1}. The chemical state of boron atoms was checked by X-ray photoelectron spectroscopy (XPS, ESCALAB 250Xi, Al Kα).

The oxidized BDAC films were physically peeled off from the substrates to obtain powders. Subsequently, 2.5 mg of the BDAC powder was placed in 0.5 mL isopropanol solution (1:3 volume ratio of isopropanol to water) and ultrasonically shaken for 1 h to obtain a BDAC suspension. The BDAC suspension was dropped onto the surface of a polished glassy carbon electrode (GCE, φ1.5 mm). Thereafter, 5 μL of Nafion solution (0.5 wt%) was placed on the electrode and dried in a dry box to obtain a working electrode. Electrochemical testing was performed on an electrochemical workstation (Shanghai Chenhua, CHI760E) using a standard three-electrode system with a Pt wire as the counter electrode and an Ag/AgCl electrode as the reference. The working electrode was mounted on a rotating disk ring electrode of the type RRDE-3A (Japan BAS). All electrochemical experiments were carried out at room temperature (25 °C).

3 Results and discussion

3.1 Physical characterization of the catalysts

Figure 1 shows SEM images of the BDAC films oxidized at 380–470 °C for 1 h. The morphology of an un-oxidized sample is also given as a comparison. It can be seen from Fig. 1 that the surface of the carbon films synthesized by HFCVD is composed of many cauliflower-like deposits, which is consistent with the typical morphological features of the amorphous carbon films. It can be also known by comparing with the un-oxidized carbon films that many holes and gaps appear on the surface after oxidizing treatments. This is because the carbon atoms in the junctions of the cellular BDAC film surface react with oxygen in the air at a faster rate, which is similar to the cracks formation on the phenolic resin-derived carbon in the air oxidation experiment by Bertran et al. [20]. As oxidation temperature increases, the gaps widen and deepen of the BDAC films gradually increases. The above-mentioned surface structure feature disappears at 470 °C oxidation temperature, as can be seen from Fig. 1f. This may be caused by an unselective oxidation at an excessive oxidation temperature.

Morphology of the undoped and doped boron carbon films deposited by HFCVD at same conditions is shown in Fig. 2a, b, respectively. It can be seen that the undoped boron film is with well facet, which is the morphology of a typical diamond film. However, after doping boron, a complete grain structure has disappeared and the deposited film has the characteristic of cauliflower-like structure. It indicates that the integrity of the growing diamond crystals is destroyed by the incorporation of boron atoms. Figure 2c shows a TEM image of the doped boron carbon film. Diffused diffractive rings state clearly that the doped boron carbon films are amorphous.

Figure 3a shows the Raman spectra of the BDAC films oxidized at different temperatures for 1 h. All the samples have evident carbon characteristic peaks around 1340 cm^{-1} (D peak) and 1580 cm^{-1} (G peak) from sp^2 hybridized carbon. The G peak is caused by the stretching vibration of all sp^2 atom pairs in the carbon ring and chain and the D peak by the breathing pattern of the sp^2 atom in

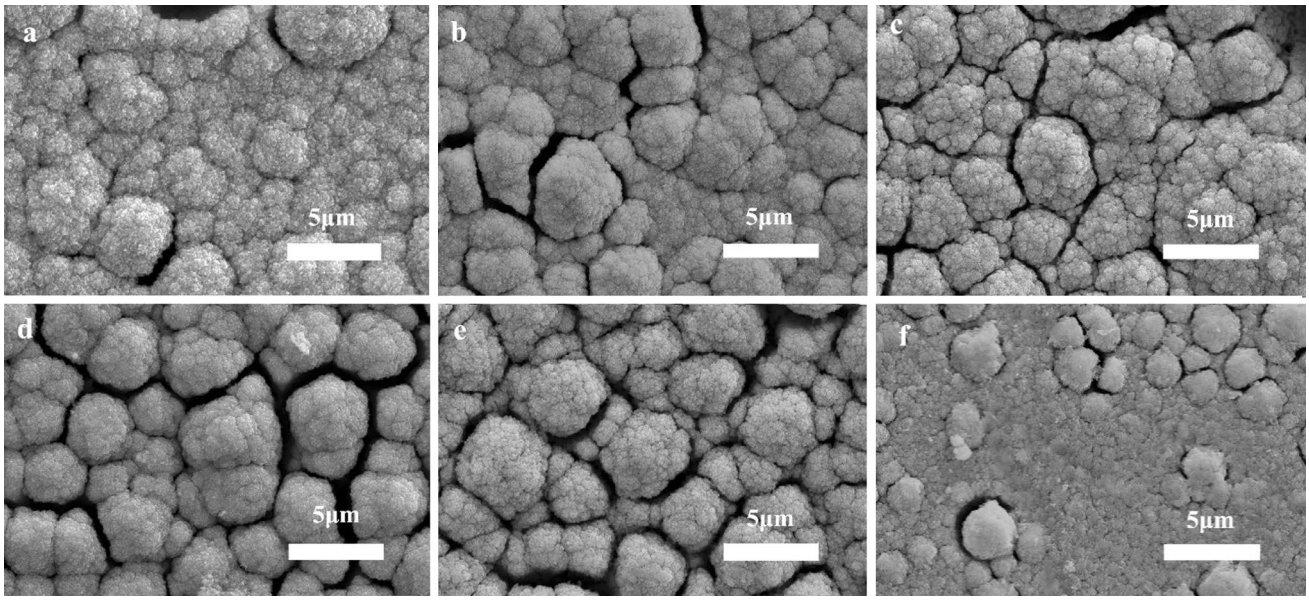

Fig. 1 SEM images of BDAC films un-oxidized (**a**) and oxidized at 380 °C (**b**), 400 °C (**c**), 430 °C (**d**), 450 °C (**e**), and 470 °C (**f**) for 1 h

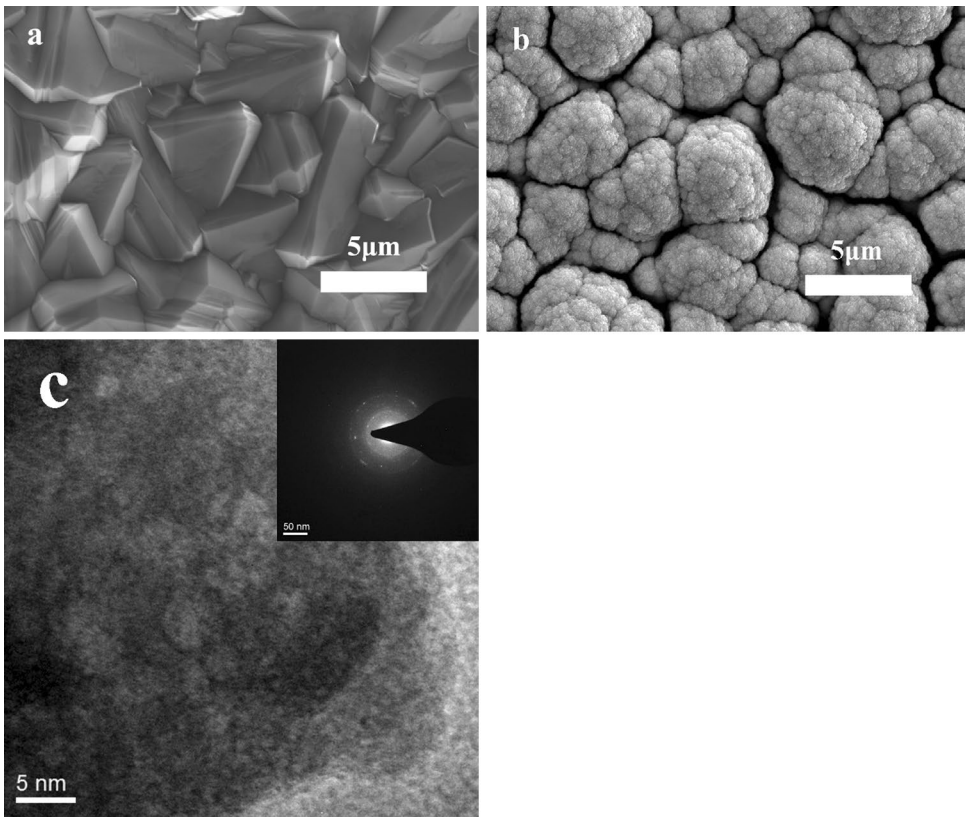

Fig. 2 SEM images of undoped (**a**) and doped boron carbon film (**b**) and HR-TEM images of the BDAC film (**c**)

the carbon ring. It is generally believed that the D and G peak represent the sp^3 hybrid and the sp^2 hybrid structure in the carbon material, respectively. Many researchers have found that when the ratio of sp^3 to sp^2 carbon is reduced, I_D/I_G is increased [21]. This is because the D and G peaks are mainly affected by the sp^2 structure and are not sensitive to changes in the sp^3 structure. Figure 3b shows the change in the integral intensity ratio obtained by fitting the D and G peaks in Fig. 3a with the oxidation temperature. As the oxidation temperature increases, the I_D/I_G

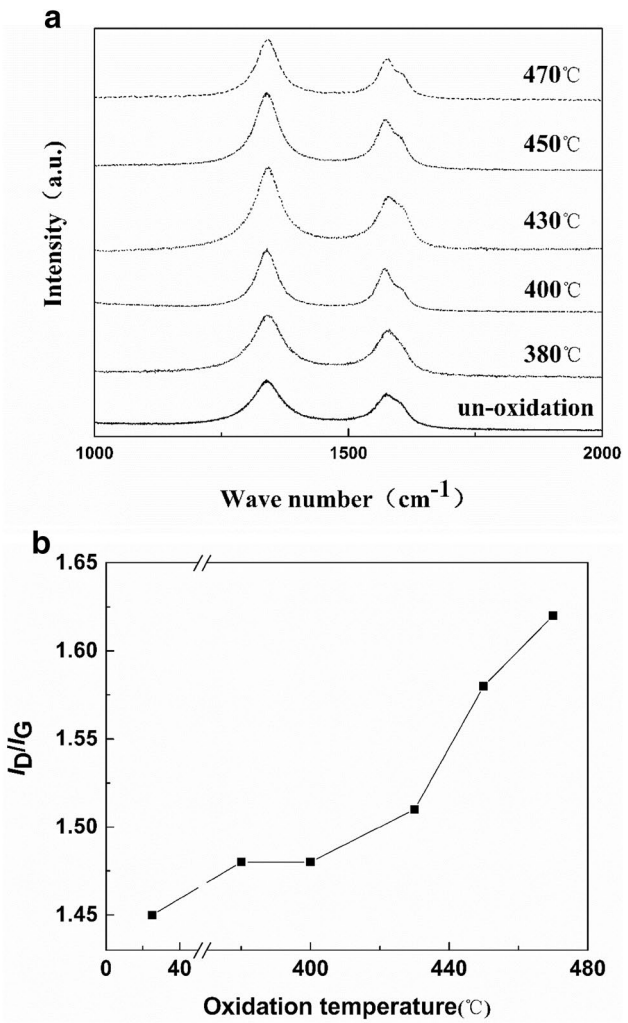

Fig. 3 Raman spectra (**a**) and I_D/I_G ratio rate (**b**) of the BDAC films oxidized at different temperatures

increases, indicating that the ratio of sp^3/sp^2 is gradually decreasing. This is because the sp^3 hybrid carbon phase is more unstable and easy to be oxidized with respect to the sp^2 hybrid carbon phase at a higher temperature. In the graphitized carbon, the sp^3 phase exists at the edge of the carbon envelope [22]. The reduction in the sp^3 hybrid carbon phase indicates that the edge of the amorphous carbon is oxidized during heat treatment, which is consistent with the increase in the gaps in the SEM observation as the oxidation temperature increases.

Figure 4 is a high-resolution XPS spectrum of the B 1s peak of an un-oxidized BDAC film. The peaks located at 186.0 and 187.3 eV in the figure represent the B–B and B–C bonds, respectively [23, 24]. The presence of the B–C bond represents the incorporation of B atoms into the carbon film and proves the atomic-level hybridization between the boron and carbon atoms.

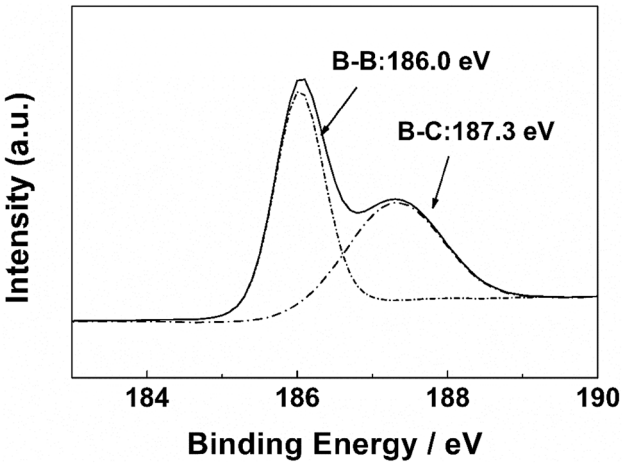

Fig. 4 High-resolution XPS spectrum for B 1s peak of the un-oxidized BDAC film

3.2 Electrochemical characterization of carbon catalysts

All the electrochemical experiments were carried out in an O_2-saturated 1 M KOH solution. The catalytic performance of the catalysts can be visually evaluated from the cyclic voltammetry (CV) curve according to the position of the oxygen reduction peak and the current density. The CV curve of the carbon films oxidized at different temperatures is shown in Fig. 5a. It can be seen that all the samples have a significant oxygen reduction peak. The oxygen reduction peak position and the peak current density also change with the oxidation temperature. Figure 5b, c, respectively, gives the variety law of the peak potential and the current density with oxidation temperature. As the oxidation temperature increases, the peak position gradually shifts to the positive direction, indicating that the oxygen reduction performance of the catalyst is enhanced. However, this enhancement is limited and the oxygen reduction potential gradually stabilizes when the annealing temperature reaches 450 °C. Meanwhile, as the oxidation temperature increases, the peak current density first increases to a maximum value at 450 °C and then decreases. It is also found that when the oxidation temperature is raised to 500 °C, the obtained BDAC films have no any catalytic performance for the ORR owing to over-oxidation.

CV curves of the catalysts of un-oxidized and oxidized at different temperatures in N_2-saturated electrolyte are shown in Fig. 6. The area of the CV curve represents the relative specific surface area of the different catalysts [25]. It is clear from Fig. 6 that the specific surface area of the catalysts increases with the increase in oxidizing temperature and reaches a maximum at 450 °C oxidizing temperature, which is consistent with the result from the SEM observation.

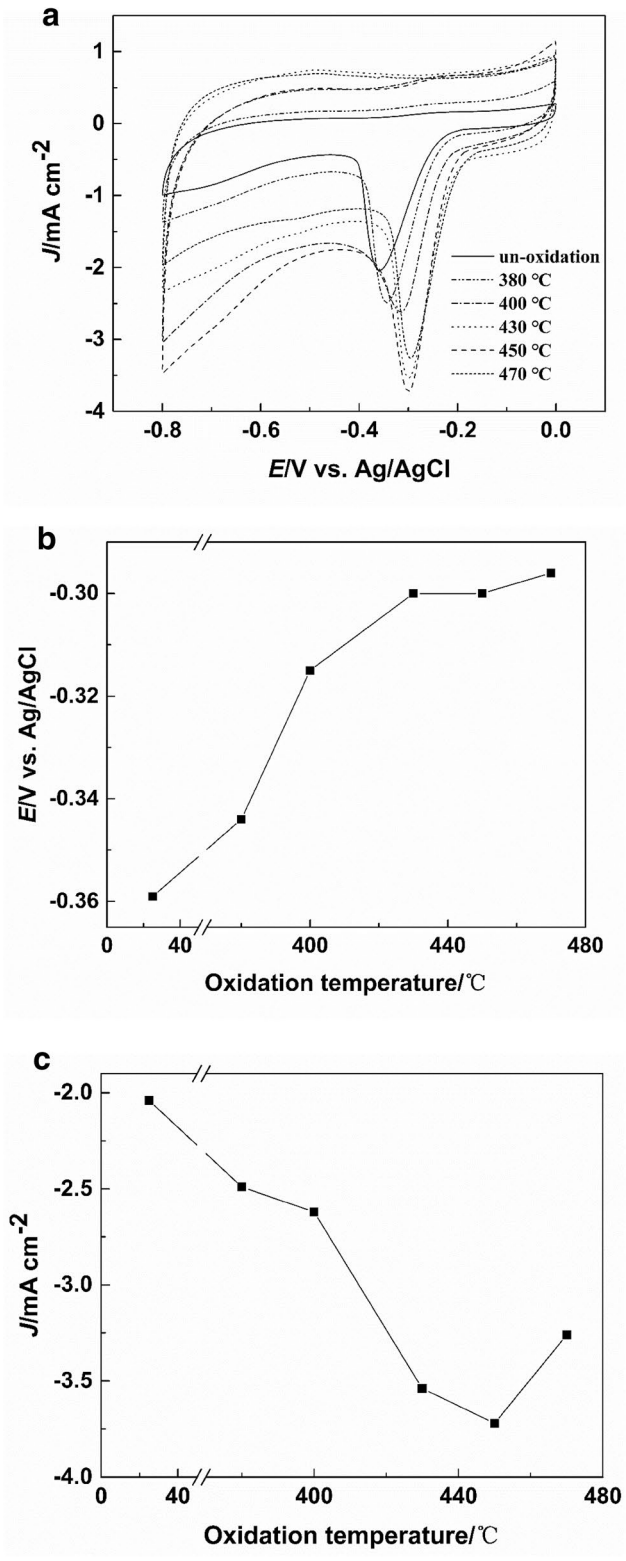

Fig. 5 Cyclic voltammetry curve (**a**), oxygen reduction peak position (**b**), and current density of the oxygen reduction peak **c** of BDAC oxidized at different temperatures

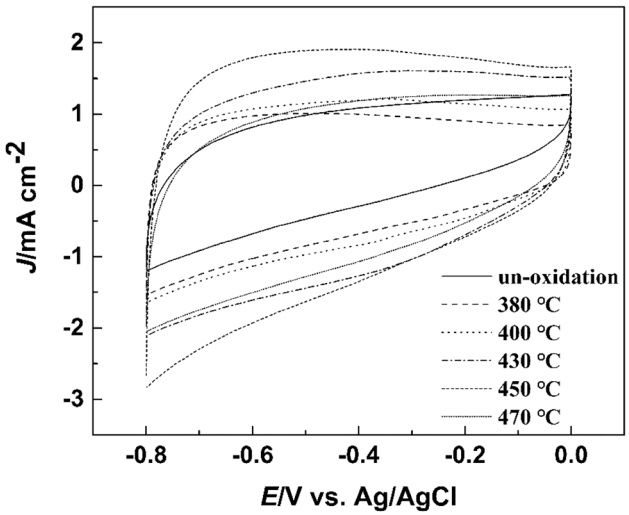

Fig. 6 CV curves of BDAC oxidized at different temperatures using a rotating disk electrode at 1600 rpm in N_2-saturated electrolyte

To further understand the catalytic performance of the BDAC films from the kinetics, linear sweep voltammetry (LSV) experiments were carried on rotating disk electrodes. Figure 7a is the LSV curves of the samples at 1400 rpm after oxidizing at different temperatures. It can be seen that the limiting current density of the un-oxidized sample is much lower than that of the annealed samples. It is clear that the oxidation treatment has a more obvious influence on the electronic structure of the BDACs and the sample oxidized at 450 °C shows the highest limiting current density. The LSV tests at rotational speeds of 600–2600 rpm were performed to clarify the catalytic performances from the kinetic aspect. The current density of the sample oxidized at 450 °C gradually increases as the number of revolutions increases, as shown in Fig. 7b. From Fig. 7b, the Koutecky–Levich point (I^{-1} vs. $\omega^{-1/2}$) at the electrode potential range from −0.40 to −0.65 V is shown in Fig. 7c and there is a good linear relationship, indicating that the catalytic process of the catalyst follows the first-order kinetics. The points of each potential are linearly fitted to obtain a K–L curve, and the curves show a certain parallelism. The number of transferred electrons n of each oxygen atom is calculated according to the K–L equation (Eq. 1) [26]:

$$I^{-1} = I_k^{-1} + \left(0.62nFCD^{2/3}v^{-1/6}\omega^{1/2}\right)^{-1} \quad (1)$$

where I is the measured current density, I_k is the kinetic current density, n is the number of electrons transferred per oxygen atom, F is the Faraday constant ($F = 96{,}485$ C mol^{-1}), C is the volume concentration of oxygen ($C = 1.2 \times 10^{-3}$ mol L^{-1}), D is the diffusion coefficient of oxygen in KOH solution ($D = 1.9 \times 10^{-5}$ cm^2 s^{-1}), v is the electrolyte dynamic viscosity ($v = 0.01$ cm^2 s^{-1}), and ω is the rotating

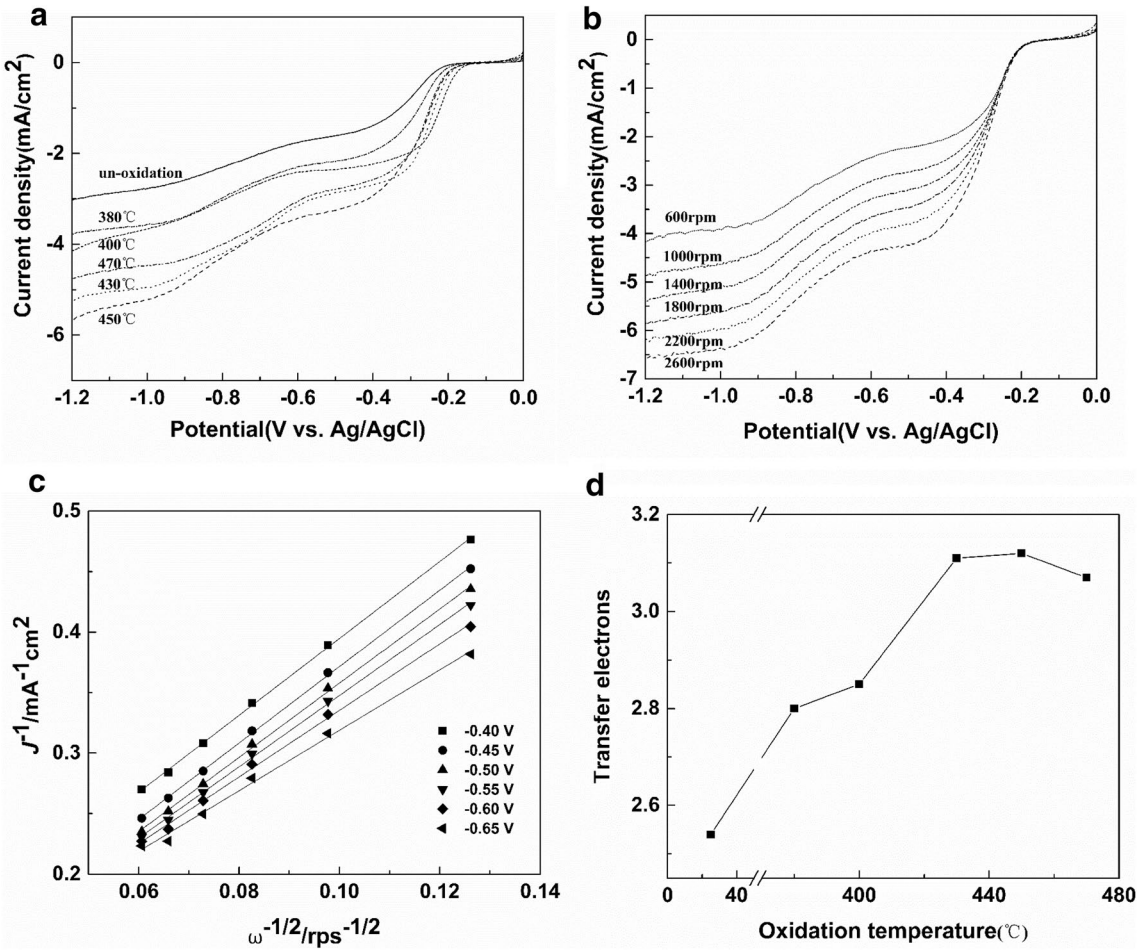

Fig. 7 **a** LSV curve obtained at a rotational speed of 1400 rpm for the samples oxidized at 25–470 °C, **b** LSV curve of the sample oxidized at 450 °C at different rotational speeds of 600–2600 rpm, **c** K–L curve of the sample oxidized at 450 °C at a potential of −0.40 to −0.65 V, and **d** number of transferred electrons versus oxidation temperature

electrode angular velocity [27]. According to Eq. (1), the number of transferred electrons at each electrode potential is obtained. The relationship between the number of transferred electrons n and the oxidation temperature is shown in Fig. 7d. The electron transfer number of the un-oxidized film is only 2.54, indicating that the ORR is mainly dominated by the two-electron reaction. With the increase in oxidation temperature, the number of transferred electrons gradually increased to a maximum value of 3.12 at 450 °C, which is consistent with the results obtained from the CV test. The number of transferred electrons n undoubtedly decreases when the temperature exceeds 450 °C. This means the ORR catalytic performance of the BDAC film oxidized around 450 °C is best.

The BDAC films were oxidized at 450 °C for 15–75 min, other being equal to determine the best oxidation time. The CV experiments are carried out, and the relationship between the oxygen reduction peak position and the oxidation time is shown in Fig. 8a. It can be seen that the oxidation time has little relationship to oxygen reduction peak position locating at −0.303 to −0.286 V. The oxidation time, however, has a great influence on the peak current density, as shown in Fig. 8b. When the oxidation time is 45 min, the current density reaches a maximum value, indicating that the catalytic performance of the sample is the best. The oxygen reduction potential of −0.286 V is very close to that of the N-doped (−0.26 V) [28] and of the P-doped carbon materials (−0.30 V) [29]. However, there is still a large gap with the potential of the commercial Pt/C catalyst (−0.14 V) [29].

The LSV tests of the samples oxidized at 450 °C for 15–75 min were also performed. The change in the number of transferred electrons with oxidation time is shown in Fig. 9. It is clear that the number of electron transfer increases first and then decreases with the increase in oxidation time. It reaches a maximum of 3.24 at 45 min oxidation time, that is to say, the catalytic performance is the best. Therefore, it has been confirmed that the optimal oxidation process is at 450 °C for 45 min.

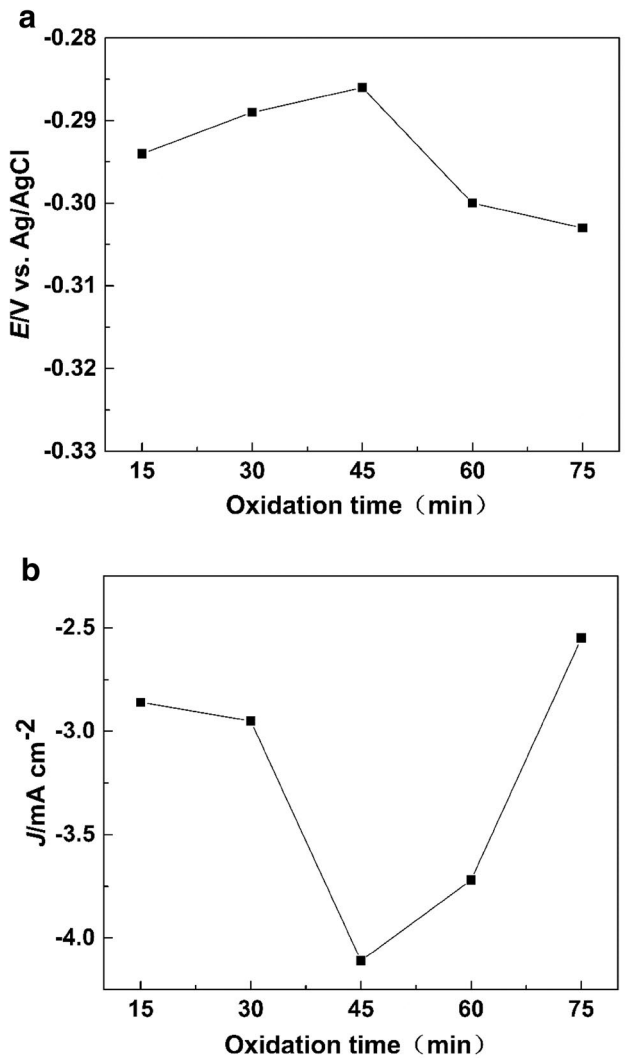

Fig. 8 **a** Peak position change of oxygen reduction; **b** change of current density of oxygen reduction peak of BDAC at different oxidation times

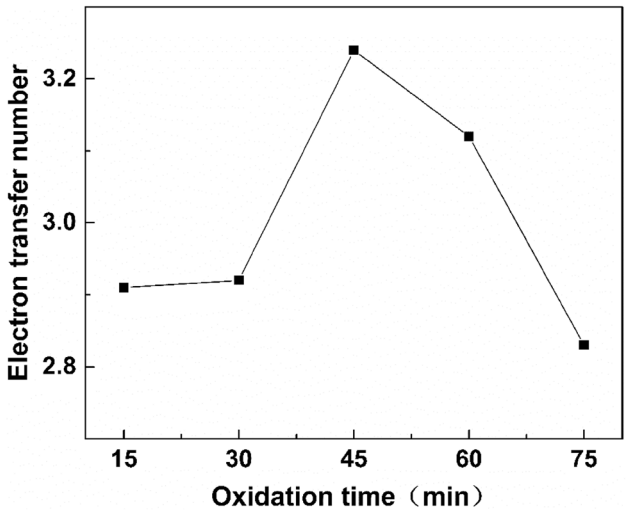

Fig. 9 Number of transferred electrons of the samples oxidized for 15–75 min

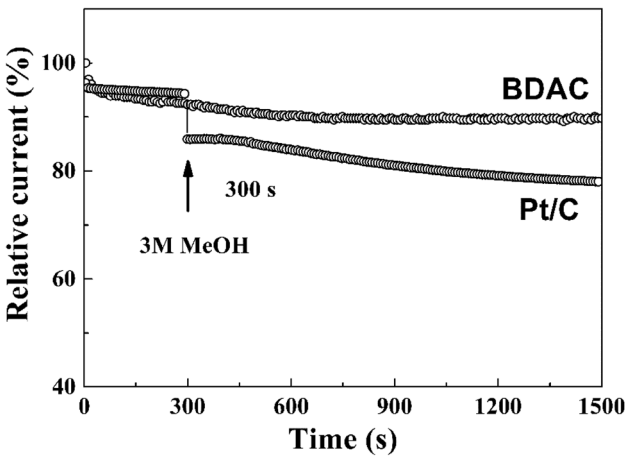

Fig. 10 Methanol resistance of Pt/C catalyst and the BDAC catalyst after oxidation at 450 °C for 1 h

In the methanol fuel cell, methanol easily passes from the anode to the cathode through the proton exchange membrane. The methanol entering the cathode will not only discharge, produce the mixing potential, and reduce the efficiency of the fuel cell, but also cause the poisoning of the cathode catalyst and reduce the catalytic performance. Therefore, methanol resistance is an important property of cathode catalysts. In the chronoamperometric test, 3 M methanol was added in the electrolyte after the ORR lasted for 300 s and then the test was continuously carried out for 1500 s. It can be seen from Fig. 10 that the current density of the BDAC catalyst has no significant decrease in the presence of methanol. The loss of current density is only 1.10% 200 s later, and the total current density only attenuates by 11.3% after adding methanol for 1500 s. As a comparison experiment, the current density of Pt/C (20% Pt) dropped sharply after the addition of methanol, as can be seen in Fig. 10. This indicates that the BDAC catalyst exhibits excellent performance in terms of resistance to methanol and has a possibility of application on a methanol fuel cell.

The durability has been investigated by the chronoamperometric i–t responses of the prepared BDAC catalyst under a constant potential of -0.28 V vs. Ag/AgCl and O_2-saturated 0.1 M KOH solution at 1000 rpm. The results are shown in Fig. 11. It is clear that a stable ORR has been sustained for 50,000 s and the loss of the ORR current density is very slight. For comparison, the durability results of sulfur-doped graphite (S-G), nitrogen-doped graphite (N-G), and Pt/C catalysts [30] for 30,000 s are also given (inset of Fig. 11). The current density loss of the S-G, N-G, and Pt/C is 27%, 35%, and 45%, respectively, and all much greater than that in

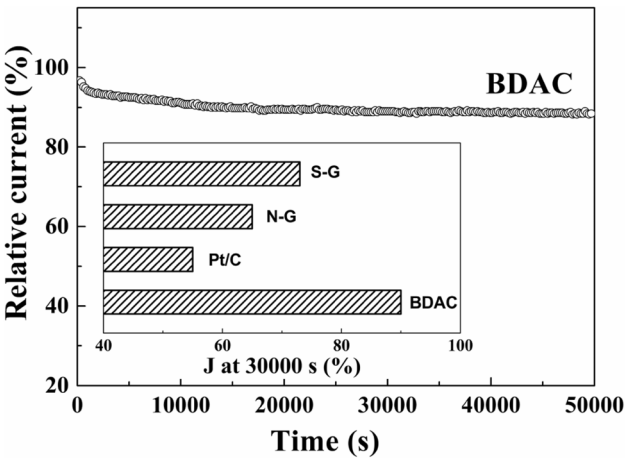

Fig. 11 Stability of Pt/C catalyst and the BDAC catalyst oxidized at 450 °C for 1 h

the present results (by 10% at 30,000 s). Moreover, the loss of the BDAC catalyst is only 11% at 50,000 s.

4 Conclusions

In summary, the effect of air oxidation on the ORR catalytic performance of BDAC films in air has been investigated. Both oxidation temperature and time have a great influence on the catalytic performance of the BDAC catalyst. It has been found that the BDAC catalyst oxidized at 450 °C for 45 min has the best catalytic performance for the ORR in an alkaline solution. Meanwhile, the treated carbon film has better methanol resistance and stability than the commercial Pt/C catalyst. The experiments have verified that this approach provides a new path to find alternatives to commercial Pt/C catalysts.

Acknowledgements This research was supported by the National Key R&D Program of China (Grant No. 2016YFB0101206), the Fundamental Research Funds for the Central Universities (DUT17ZD101), and the National Natural Science Foundation of China (NSFC 51171033).

References

1. Canadell JG, Le Quéré C, Raupach MR, Field CB, Buitenhuis ET, Ciais P et al (2007) Contributions to accelerating atmospheric CO_2 growth from economic activity, carbon intensity, and efficiency of natural sinks. Proc Natl Acad Sci U S A 104:18866
2. Shafiee S, Topal E (2009) When will fossil fuel reserves be diminished? Energy Policy 37:181
3. Möbius HH (1997) On the history of solid electrolyte fuel cells. J Solid State Electrochem 1:2
4. Debe MK (2012) Electrocatalyst approaches and challenges for automotive fuel cells. Nature 486:43
5. Zheng Y, Jiao Y, Jaroniec M, Jin Y, Qiao SZ (2012) Nanostructured metal-free electrochemical catalysts for highly efficient oxygen reduction. Small 8:3550
6. Wang L, Wurster P, Gazdzicki P, Roussel M, Sanchez DG, Guétaz L et al (2018) Investigation of activity and stability of carbon supported oxynitrides with ultra-low Pt concentration as ORR catalyst for PEM fuel cells. J Electroanal Chem 819:312
7. Wang Z, Zhu Y, Luo W, Ren Y, Cheng X, Xu P et al (2016) Controlled synthesis of ordered mesoporous carbon-cobalt oxide nanocomposites with large mesopores and graphitic walls. Chem Mater 28:7773
8. Gao S, Fan B, Feng R, Ye C, Wei X, Liu J, Bu X (2017) N-doped-carbon-coated Fe_3O_4 from metal-organic framework as efficient electrocatalyst for ORR. Nano Energy 40:462
9. Lai Q, Zheng L, Liang Y, He J, Zhao J, Chen J (2017) Metal–organic-framework-derived Fe-N/C electrocatalyst with five-coordinated Fe-N_x sites for advanced oxygen reduction in acid media. ACS Catal 7:1655
10. Huang B, Peng L, Yang F, Liu Y, Xie Z (2017) Improving ORR activity of carbon nanotubes by hydrothermal carbon deposition method. J Energy Chem 26:712
11. Lehmann K, Yurchenko O, Melke J, Fischer A, Urban G (2018) High electrocatalytic activity of metal-free and non-doped hierarchical carbon nanowalls towards oxygen reduction reaction. Electrochim Acta 269:657
12. Liu L, Zeng G, Chen J, Bi L, Dai L, Wen Z (2018) N-doped porous carbon nanosheets as pH-universal ORR electrocatalyst in various fuel cell devices. Nano Energy 49:393
13. Rybarczyk MK, Gontarek E, Lieder M, Titirici MM (2018) Salt melt synthesis of curved nitrogen-doped carbon nanostructures: ORR kinetics boost. Appl Surf Sci 435:543
14. Gong J, Lin H, Antonietti M, Yuan J (2016) Nitrogen-doped porous carbon nanosheets derived from poly (ionic liquid) s: hierarchical pore structures for efficient CO_2 capture and dye removal. J Mater Chem A 4:7313
15. Ling Z, Wang Z, Zhang M, Yu C, Wang G, Dong Y et al (2016) Sustainable synthesis and assembly of biomass-derived B/N co-doped carbon nanosheets with ultrahigh aspect ratio for high-performance supercapacitors. Adv Funct Mater 26:111
16. Zhang L, Qi C, Zhao A, Xu G, Xu J, Zhang L et al (2018) N-doped porous carbon-encapsulated Fe nanoparticles as efficient electrocatalysts for oxygen reduction reaction. Appl Surf Sci 445:462
17. Zhong W, Chen J, Zhang P, Deng L, Yao L, Ren X, Li Y, Mi H, Sun L (2017) Air plasma etching towards rich active sites in Fe/N-porous carbon for the oxygen reduction reaction with superior catalytic performance. J Mater Chem A 5:16605. https://doi.org/10.1016/j.apsusc.2018.03.145
18. Wiener M, Reichenauer G (2015) Microstructure of porous carbons derived from phenolic resin-Impact of annealing at temperatures up to 2000 °C analyzed by complementary characterization methods. Microporous Mesoporous Mater 203:116
19. Gokuladeepan P, Karthigeyan A (2018) Effect of annealing temperature on oxygen reduction reaction of reduced graphene oxide incorporated cobalt oxide nanocomposites for fuel cell applications. Appl Surf Sci 449:705
20. Bertra X, Chollon G, Dentzer J, Gadiou R, Fouquet S, Dourges MA, Rebillat F (2017) Oxidation behavior at moderate temperature under dry and wet air of phenolic resin-derived carbon. Thermochim Acta 649:13
21. Ferrari AC, Robertson J (2000) Interpretation of Raman spectra of disordered and amorphous carbon. Phys Rev B 61:14095
22. Shen A, Zou Y, Wang Q, Dryfe RA, Huang X, Dou S, Dai L, Wang S (2014) Oxygen reduction reaction in a droplet on graphite: direct evidence that the edge is more active than the basal plane. Angew Chem 126:10980

23. Shirasaki T, Derré A, Ménétrier M et al (2000) Synthesis and characterization of boron-substituted carbons. Carbon 38:1461
24. Zhao Y, Yang L, Chen S et al (2013) Can boron and nitrogen co-doping improve oxygen reduction reaction activity of carbon nanotubes? J Am Chem Soc 135:1201
25. Zhang X, He W, Zhang R et al (2016) High-performance carbon aerogel air cathodes for microbial fuel cells. Chemsuschem 9:2788
26. Shao Y, Yin G, Gao Y (2007) Understanding and approaches for the durability issues of Pt-based catalysts for PEM fuel cell. J Power Sources 171:558
27. Chen W, Chen S (2009) Oxygen electroreduction catalyzed by gold nanoclusters: strong core size effects. Angew Chem 121:4450
28. Liu R, Wu D, Feng X, Müllen K (2010) Nitrogen-doped ordered mesoporous graphitic arrays with high electrocatalytic activity for oxygen reduction. Angew Chem 122:2619
29. Liu ZW, Peng F, Wang HJ, Yu H, Zheng WX, Yang J (2011) Phosphorus-doped graphite layers with high electrocatalytic activity for the O_2 reduction in an alkaline medium. Angew Chem Int Ed 50:3257
30. Yang S, Zhi L, Tang K, Feng X, Maier J, Müllen K (2012) Efficient synthesis of heteroatom (N or S)-doped graphene based on ultrathin graphene oxide-porous silica sheets for oxygen reduction reactions. Adv Funct Mater 22:3634